PROCEEDINGS, 41st Workshop on Geothermal Reservoir Engineering
Stanford University, Stanford, California, February 22-24, 2016
SGP-TR-209

Development of an Ultrasonic Phased Array System for Wellbore Integrity Evaluation and Near-Wellbore Fracture Network Mapping of Injection and Production Wells in Geothermal Energy Systems*

Hector J. Santos-Villalobos[1], Christi Johnson[1], Case Collins[1], Hani Abdulrahman[2], Benjamin Foster[2], Roger Kisner[1], Yarom Polsky[1], and Charles Bouman[2]

[1]Oak Ridge National Laboratory, One Bethel Valley Road MS-6075, Oak Ridge, TN 37831
[2]Purdue University, MSEE 320, 465 Northwestern Avenue, West Lafayette IN 47907-2035

[1]hsantos@ornl.gov, [2]bouman@purdue.edu

Keywords: Ultrasound, NDE, Non-Destructive Evaluation, Computational Imaging, Image Reconstruction, Model-Based Iterative Reconstruction, MBIR

ABSTRACT

This paper documents our progress developing an ultrasound phased array system in combination with a model-based iterative reconstruction (MBIR) algorithm to inspect the health of and characterize the composition of the near-wellbore region for geothermal reservoirs. The main goal for this system is to provide a near-wellbore in-situ characterization capability that will significantly improve wellbore integrity evaluation and near well-bore fracture network mapping. A more detailed image of the fracture network near the wellbore in particular will enable the selection of optimal locations for stimulation along the wellbore, provide critical data that can be used to improve stimulation design, and provide a means for measuring evolution of the fracture network to support long term management of reservoir operations. Development of such a measurement capability supports current hydrothermal operations as well as the successful demonstration of Engineered Geothermal Systems (EGS). The paper will include the design of the phased array system, the performance specifications, and characterization methodology. In addition, we will describe the MBIR forward model derived for the phased array system and the propagation of compressional waves through a pseudo-homogenous medium.

1. INTRODUCTION

Controlled engineering of the subsurface requires detailed structural and material characterization of the wellbore and near-wellbore regions because these are the general initiation and access points of our subsurface manipulations. This applies to all subsurface energy related applications including geothermal energy extraction, oil & gas production, carbon sequestration and deep borehole disposable of nuclear waste. Use of this characterization information falls into two general categories: 1) Monitoring of the current and evolving state of the wellbore and reservoir in order to confirm that operations are under control, and 2) Definition of geomechanical inputs needed in order to manipulate the reservoir to desired effect. For example, with respect to the former, breaches of zonal isolation can have effects ranging from zonal communication that adversely effect fluid production to complete wellbore integrity compromise that results in aquifer contamination or surface emission. These breaches are often a result of structural and material issues such as casing corrosion, cement voids, delamination between the casing and cement or casing and rock, cement fractures and cement degradation, but are in many instances difficult to measure (Gasda, 2004). With respect to the latter, it is generally recognized that spatial characteristics and distribution of fractures in the reservoir have a tremendous impact on permeability creation and behavior. This is the impetus for the huge focus over the last few years on the development of discrete element approaches for explicitly modeling fluid driven propagation of fractures.

While there has been significant advancement of the tools that are available to characterize the features of interest in these regions (Gaillot, 2007), much progress remains to be made if a more comprehensive and detailed characterization of the environment is desired. State of the art commercial offerings such as cement bond logging and ultrasonic imaging tools tend to have resolutions limitations dictated by practical considerations. Increased resolution, for example, can be obtained by increasing the frequency of the interrogating ultrasound, but at the expense of signal intensity and range of measurement because ultrasound attenuation is generally proportional to the square of sound frequency. Increases of resolution also incur larger computational costs for image reconstruction, making high fidelity physics-based reconstruction methods infeasible for real-time logging applications. These difficulties associated with sound propagation and reconstruction also limit the applicability of interrogation of the near wellbore region where acoustical impedance mismatches and material heterogeneity present enormous challenges. Consequently, it is common in both the geothermal and oil & gas industries to rely on acoustic televiewer logs of the borehole face along with expert interpretation to develop a model of the fracture distribution within the reservoir. Unfortunately, this approach has not been able to resolve fractures of smaller aperture (<1mm) when compared with core samples from measured intervals (Genter, 1997).

In order to address the inherent challenges of nondestructive assessment of the health and structure of the wellbore and the near-wellbore region, we are developing an ultrasonic phased array and a hardware-tailored model-based iterative reconstruction (MBIR) algorithm (Thibault et al., 2007). The phased array system increases signal to noise ratio and provide unique measurements of the specimen from multiple simultaneous viewpoints while MBIR offers a framework to reach high quality reconstructions from sparse, noisy data by the use of *a priori* information about the specimen under interrogation. The next section provides a primer on MBIR and documents the current status of our MBIR implementation for ultrasound signals—including the forward model, the a priori model, and the optimization algorithm. Then, we discuss the specifications of the phased array system and our transducer characterization methodology. Then, we document the scanning and reconstruction strategy and how the ultrasonic phased array and the MBIR algorithm work together. We conclude the paper with final remarks and future work.

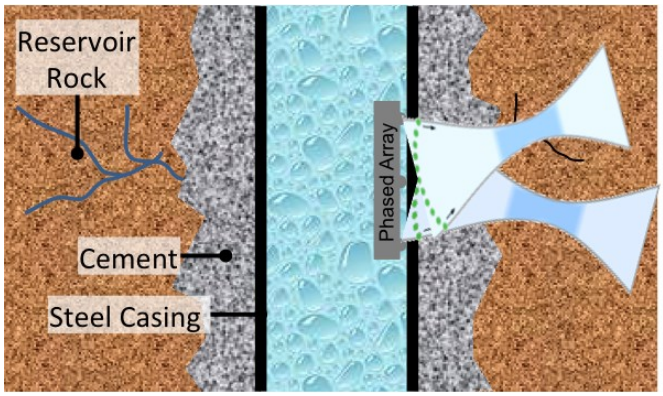

Figure 1: Illustration of geothermal well components, a few near wellbore features of interest, and phased array system. The figure also illustrates the capability of phased array system to steer the acoustic wavefront different directions from the same position.

2. MODEL-BASED ITERATIVE RECONSTRUCION

Model-Based Iterative Reconstruction (MBIR) is a family of iterative reconstruction techniques that has three important components: 1) modeling of physical system $f(x)$, which includes the signal modality (e.g., visible light, x-ray, sound, etc.), medium interaction/propagation (e.g., signal attenuation, scattering, reflections, refraction, etc.), and the measurement system properties (e.g., source intensity, source beam profile, sensitivity, etc.); 2) *a priori* model $p(x)$, which establishes the rules and parameters to penalize object estimates that depart from the expected object values.; and 3) the cost function, which estimates the error between the actual system measurements and the synthetic measurements generated by the MBIR model given an object estimate x. Figure 2 illustrates the reconstruction workflow. The geothermal well is the object x to image and the ultrasonic phased array is the physical measurement system from which several measurement $\boldsymbol{y}$ are obtained. The object x is a discretized version of the real object, where for a pre-determined resolution each space coordinate is indexed to a cell or pixel. After obtaining the measurements, the reconstruction process initiate. Typically, the object pixels are initialized to zero or set by a previous lower quality reconstruction. Then, synthetic measurements are generated from the physical system model given an object estimate. These synthetic measurements are compared against the real measurements y. Then, the object estimate is updated given the error cost computed in the previous step. Consequently, the updated object is passed to the prior model to penalize pixels that break the expected values for its pixel neighborhood or that are outside the expected range. It is important to emphasize that these unexpected values are penalized or discouraged, but not truncated or forced to the expected value. This iterative process will continue until the cost function is below a predetermined value or until a desired number of iterations is performed.

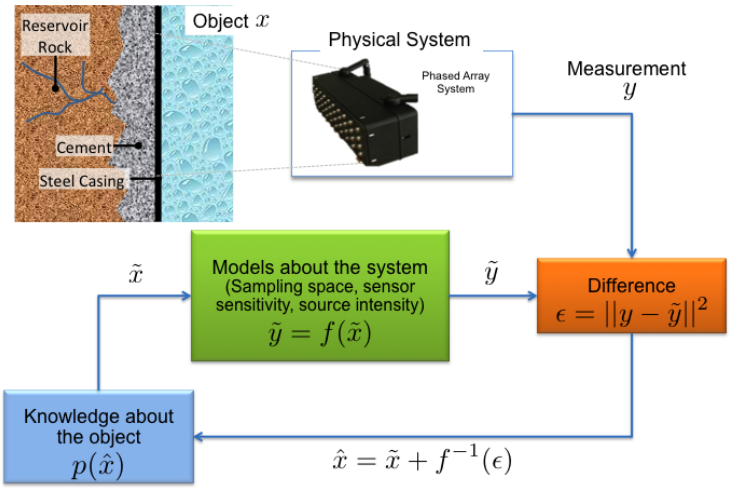

Figure 2: Illustration of iterative reconstruction workflow for MBIR. The top components represent the real world and measurement system, while the bottom boxes represent the computer algorithm used in the reconstruction of the object.

2.1 MBIR overview

The following is a brief documentation of our use of Maximum A Posteriori (MAP) estimation / MBIR techniques for the reconstruction of ultrasonic signals. Suppose, we have some data *Y,* and that we know of some transformation *A* that maps the data *Y* to some desired but unknown signal X. That is,

$$Y = AX \tag{1}$$

In addition, it may be the case that our data can be modeled as being noisy (i.e., there is some additive component *W* of the transformation from X to Y). Then,

$$Y = AX + W \tag{2}$$

If we additionally assume that *Y* and *X* are random quantities, then we must use techniques from probability and estimation theory in order to find a defensible estimate of *X*. As mentioned earlier, we would like to impose conditions on *X* that enforce spatial regularity, among other attributes. We can incorporate this type of condition in an estimation-theoretical manner by making use of Bayes' theorem:

$$p_{x|y}(x \mid y) = \frac{p_{y|x}(y \mid x) p_x(x)}{p_y(y)} \tag{3}$$

From this version of Bayes' rule, we are able to derive the MAP estimate of *X* given *Y*:

$$\hat{X}_{MAP} = \underset{x}{\operatorname{argmax}} \left\{ \log(p_{y|x}(y \mid x)) + \log(p_x(x)) - \log(p_y(y)) \right\} \tag{4}$$

or equivalently:

$$\hat{X}_{MAP} = \underset{x}{\arg\min} \left\{ \log(p_{y|x}(y \mid x)) + \log(p_x(x)) \right\} \tag{5}$$

since the probability distribution function of *Y* does not depend on *X* and the functions are valid probability density functions. The first term on the right-hand side of this expression is called the likelihood function, and describes the probabilistic relationship between the data *Y* and the desired object estimate *X*; this the physical system model in Figure 2 and it will be defined shortly. The second term is the prior model shown in Figure 2. We choose to impose a prior model called the Q-Generalized Gaussian Markov Random Field (QGGMRF) model, which works to both promote smoothness in low-frequency regions of an image and preserve edges in high-frequency regions of an image (Kisner et al., 2012).

For most applications, solving the MAP function in its closed form may be unfeasible. The MAP function can be represented as a system of equations, where the coefficients of the equations form a matrix *A*. (Shortly, we will discuss how we compute the forward model and *A*.) In order to solve the system of equations in its closed form, we need to compute the inverse of *A*. However, it is not guaranteed that *A* is square and invertible or the matrix may be too large to be stored in a computer. In addition, it is not certain that the prior term will admit a solution in closed form. Consequently, we must resort to iterative numerical optimization techniques, such as

Conjugate Gradient Descent (Møller, 1993) and Iterative Coordinate Descent (ICD) (Friedman et al., 2010). In our case, ICD minimization is used to solve the minimization problem posed in the previous paragraph.

2.1 Designing the forward model $p_{y|x}$

We were successfully able to design a simple forward model for acoustic system. This model was made with certain assumptions to make reconstruction easier for first stage MBIR. The goal is to eliminate each assumption as we proceed further with the project. The assumptions are as follows: constant acoustic speed, homogenous medium, isotropic medium, Born approximation, and coherent integration (Norton and Linzer, 1981).

$$y_{i,j}(t) = \int y_{i,j}(t,p)\,dp \tag{6}$$

$$y_{i,j}(t,p) = \int A_{i,j}(T_{i,j}(p),t)\,x(p)\,dp \tag{7}$$

$$A_{i,j}(T_{i,j}(p),t) = \mathrm{h}_{i,j}(T_{i,j}(p), t - T_{i,j}(p)) \tag{8}$$

$$\mathrm{h}_{i,j}(T_{i,j}(p),t) = F^{-1}\left\{ \tau_1^2 \tau_2^2 S(f) \mathrm{e}^{-\alpha_0 c |f| T_{i,j}(p)} \right\} \tag{9}$$

$$T_{i,j}(p) = \frac{\|p - r_i\| + \|p - r_j\|}{c} \tag{10}$$

where t is time in seconds, $y_{i,j}(t)$ is the output of the system for transmitter i and receiver j, p is the position of the object pixel in 3-dimensional space, $x(p)$ is the reflection coefficient that we want to reconstruct, F^{-1} is the inverse Fourier transform, τ is the transmittance coefficient of the medium, $s(t)$ is the input signal, α_0 is the attenuation coefficient in decibels per meter Hz, and c is the speed of sound in meters per second. Note that when the medium is isotropic a single transmitter/receiver pair cannot discriminate the pixel that caused a received reflection. Given time of flight laws, the received reflection can be produced at any pixel p with equal path length from transducer i to pixel p to transducer j. This fact is exploited in Equation 5 to reduce the cost of computing the system matrix A. The forward model was implemented in Matlab. The code generates the matrix A, which is used along with the measurements data y as inputs to the MBIR algorithm to reconstruct the image. Full documentation of the discretization of the forward model can be found at Almansouri et al. (2015).

3. ULTRASOUND PHASED ARRAY SYSTEM

An ultrasonic phased array system composed of sixteen piezoelectric composite transducers and a sixteen channel phased array pulser/receiver board with delay capabilities down to 1.5 nanoseconds is being used for laboratory study of the imaging method being developed. . The transducers have a central frequency response around 100 kHz and broad bandwidth of 48 kHz. The wide bandwidth will allow resolution of features smaller than half the wavelength provided by the central frequency and the future application of additional image processing techniques to improve resolution and SNR, such as wavelet decomposition. There are several reasons to select a phased array approach for the measurement system. First, the focusing of ultrasonic phased arrays is well documented in the scientific and commercial literature (Hynynen et al. 2004, Shattuck et al. 1987). This feature increases the intensity of the signals at the focus point by a factor of N^2, where N is the number of transducers in the array. This ability to project energy deeper into highly attenuating media is critical when imaging thick specimens like the near wellbore region. Second, the wave front produced by the phased array system can be steered in order to provide distinct measurements from the same viewpoint. This is important for MBIR, because it increases the rank of the system model matrix A. Third, different acoustic patterns can be generated. For example, as shown in the next section, only a few transducers can be activated to image regions close to the surface while more transducers can be activated for deeper regions.

Figure 3: The image at the left shows the time domain and frequency response of a transducer pair after the transmitter is excited with a 1 cycle, 10 Vpp, 100 kHz, sine-shaped pulse. The plot at the bottom of the graph shows the frequency

response, which has a 95 kHz center frequency and 48 kHz bandwidth. The image at the right shows two Ultran Group GRD100-D19 transducers configured for an empirical estimation of signal amplitude.

One important element for MBIR reconstruction is to properly model the physical measurement system. For transducers this is a challenging task. The point spread function of the transducer source changes with couplant material, transducer/sample surfaces contact pressure, surface roughness, orientation of transducer surface with respect to sample surface, and the sample material. Therefore, as we move away from the isotropic assumption, we need to empirically measure the complete signal response of a transducer pair (transmitter and receiver). The goal is to generate characterization models that are sample agnostic. For example, the right image in Figure 3 shows a transducer pair configured for signal amplitude characterization. By using the approach, we can model the relative signal intensity across our transducers for later signal amplitude scaling and normalization. Note that such a measurement gives little information about the actual intensity/sensitivity profile of the transducers. As show in Figure 4 (a), there is a cone-shaped area for the transducer source (e.g., green cone) where the intensity of the signal will be the strongest at the center and weakest at the periphery. Likewise, the receiver sensitivity is strongest for waves with incidence angle orthogonal to the transducer surface and less sensitive for steep incident angles. Figure 4 (b) shows a picture of the setup used to capture the full signal profile. A transmitter is placed at one side control sample and a receiver is placed at the other side. Following the position pattern shown in Figure 4 (c), we position the receiver at an angle from the source in order to capture changes in intensity and sensitivity for a transducer pair. This process needs to be performed for all transducer pairs. These measurements are important for normalization of the phased array system transducers relative to each other.

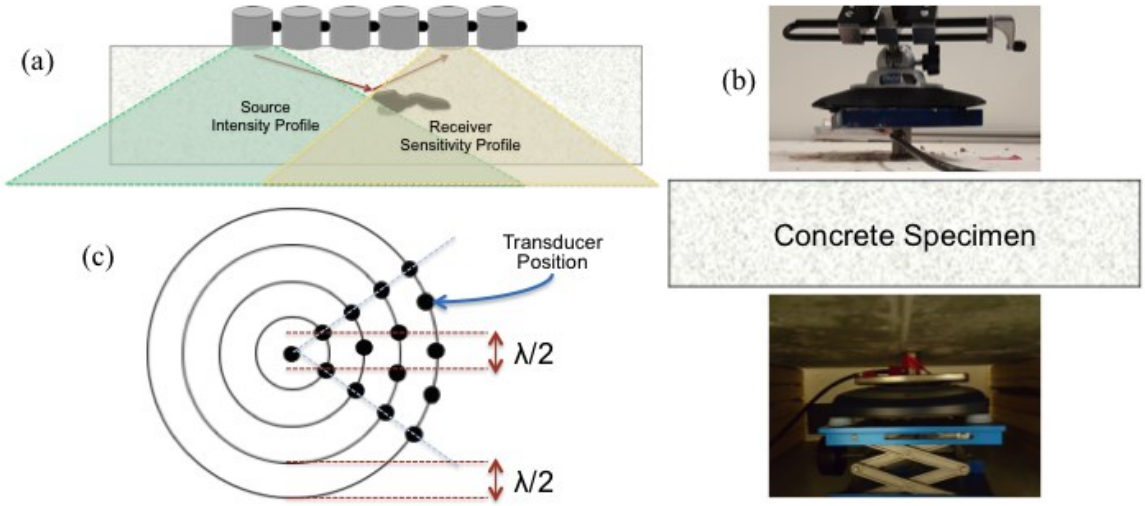

Figure 4: Transducer characterization images. (a) Transmitter and receiver intensity and sensitivity profile. (b) Setup of a transmitter (bottom) and a receiver (top) on opposite sides of a control cement slab. (c) Position pattern for the receiver in (b).

3. SCANNING AND RECONSTRUCTION STRATEGY

The algorithm under development is inspired by previous work on medical X-ray Computed Tomography (CT) (Kisner et al., 2012) and 3D bright field electron tomography (Singanallur et al., 2014). In contrast to ultrasonic waves, which are mechanical waves, X-rays are electromagnetic waves. Both modalities follow the Beer-Lambert Law. However, ultrasound waves add the challenge of mode conversion and strong reflections due to impedance differences. For X-rays, reflections at material changes can be discarded. This is not the case for acoustic imaging. Therefore, the propagation model needs to take in account the attenuation of the signal due to scattering and other factors such as a spreading and signal loss due to reflections at interfaces with impedance changes. To work around this challenge and still employ the forward model proposed above, we plan to implement a progressive scanning/reconstruction approach, as shown in Figure 5. In Figure 5, (a) shows the reconstruction workflow and (b) illustrates the concept inside the well.

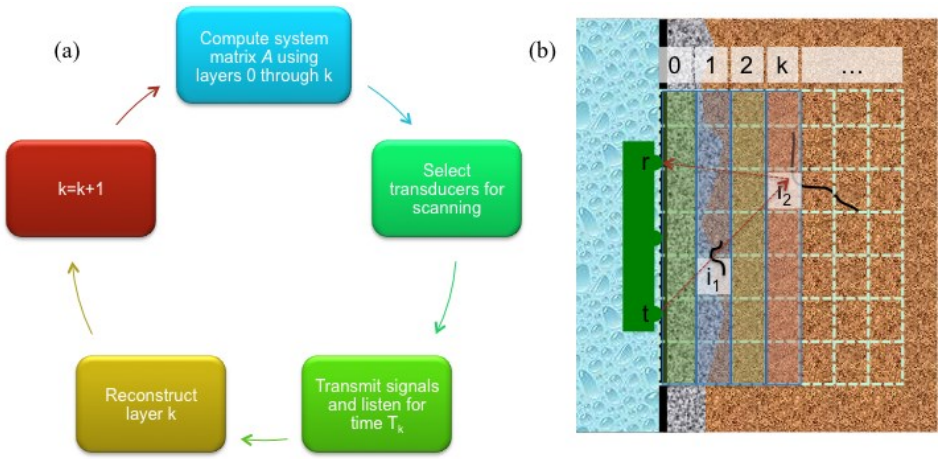

Figure 5: Illustration of progressive scanning/reconstruction technique. (a) Reconstruction workflow. (b) The progressive scanning reconstruction approach first reconstructs signals from shallow regions and progressively listens and reconstruct signals deeper into the rock formation.

The progressive scanning process works as follows: First, the specimen is discretized in cells no greater than half the wavelength of the system and a system matrix A is computed for the first layer (i.e., k=0). Transducer selection is limited to transmitter/receiver pairs with a wave path that does not exceed the depth of the current layer. This is achieved by controlling the time to listen for reflections. The receivers listen for a time T_k based on the time it takes the ultrasonic wave to reach the back of the current layer k and return to the receiver. Note that for shallower layers, it may be necessary to disable the phased array mode, because the wave paths for transducers at the periphery may exceed the constraints imposed above. However, as we move to deeper layers, all transducers can be utilized and only T_k controls the reconstruction depth. After the signals are received, the layer k is reconstructed and the system prepares for the reconstruction of the next layer. Note that the time delays for phased array wave front steering and focusing could be adjusted based on the new information learned about the specimen in order to increase SNR. In addition, the computation of the new matrix A takes in account reflections discovered at the previous layer. This point is illustrated in Figure 5 (b). Note that the intensity of the reflection received at transducer r should include losses for the attenuation for traveling from transducer t to point i_2, to transducer r, and the reflection and transmission at points i_1 and i_2, respectively. The reflection at point i1 is not taken in account by our forward model in Equation 6. By progressively reconstructing the specimen, we can take in account these early reflections in a new system matrix and improve reconstruction quality.

4. CONCLUSIONS

We currently have a Matlab implementation of the MBIR forward model, QGGMRF prior model, and the ICD optimization algorithm. The current version of the algorithm had been tested with synthetic phantoms. We are currently enhancing the software to include the progressive scanning/reconstruction approach. In addition, we are prepared for laboratory experiments. We fabricated three 3x3x1 cubic feet cement slabs, which include a control slab (i.e., pure cement), a slab with a steel plate embedded, and a third slab with a steel plate and a ball embedded. The third slab is the more challenging sample; given that the steel plate is suppose to occlude the steel ball behind it. In addition, we have acquired preliminary ultrasonic data sets of the laboratory samples using the 16-transducer array. After the reconstruction algorithm progressive method is implemented, we will assess the performance of MBIR against conventional time of flight reconstruction methods.

In this paper, we have documented our progress developing an ultrasound phased array system for the assessment of the health of geothermal wells and for the characterization of the near-wellbore region. The method includes the implementation of a Model-Based Iterative Reconstruction algorithm for ultrasonic signals. We had documented our progress designing the phased array system, the characterization methodology, the initial forward model for MBIR, and the scanning/reconstruction strategy. In the future, we plan to continue improving the forward model. For example, mode conversion (i.e., p-wave to s-wave conversion) or wave diffraction was not addressed in the current forward model. In addition, we plan to document the empirical performance of the system and reconstruction algorithm for laboratory samples.

5. ACKNOWLEDGMENTS

This research was supported by the U.S. Department of Energy's Subsurface Technology and Engineering Research, Development, and Demonstration (SubTER) Technology Team.

6. REFERENCES

Almansouri, H., Clayton. D., Kisner, R., Polsky, Y., Bouman, C., and Santos-Villalobos. H.: Development of Acoustic Model-Based Iterative Reconstruction Technique for Thick Concrete Imaging, *Proceedings,* 42nd Annual Review of Progress in Quantitative Nondestructive Evaluation, Center for Nondestructive Evaluation Iowa State University, Minneapolis, Minnesota (2015).

Friedman, J., Hastie T., and Tibshirani, R.: Regularization paths for generalized linear models via coordinate descent, *Journal of Statistical Software,* **33**, (2010), 1.

Gaillot, P., Brewer, T., Pezard, P., and Yeh, E.: Borehole Imaging Tools - Principles and Applications, *Scientific Drilling*, **5**, (2007), 1-4.

Gasda, S.E., Bachu S. and Celia, M.A.: Spatial Characterization of the Location of Potentially Leaky Wells Penetrating a Deep Saline Aquifer in a Mature Sedimentary Basin, *Env. Geol.*, **46**, (2004), 707-720.

Genter, A., Castaing, C., Dezayes, C. Tenzer, H., Traineau, H., and Villemin, T.: Comparative Analysis of Direct (Core) and Indirect (Borehole Imaging Tools) Collection of Fracture Data in the Hot Dry Rock Soultz Reservoir (France), *J. Geophys. Res*., **102**, (1997), 15,419-15,431.

Hynynen, K., Clement, G.T., McDannold, N., Vykhodtseva, N., King, R., White, P.J., Vitek, S. and Jolesz, F.A.: 500-Element Ultrasound Phased Array System for Noninvasive Focal Surgery of the Brain: A preliminary Rabbit Study With Ex Vivo Human Skulls, *Magnetic Resonance in Medicine*, **52**, (2004), 100-107.

Kisner, S. J., Haneda, E., Bouman, C. A., Skatter, S., Kourinny, M., and Bedford, S.: Limited view angle iterative CT reconstruction, *Proceedings,* IS&T/SPIE Electronic Imaging, International Society for Optics and Photonics, San Francisco, CA (2012).

Møller, M. F.: A scaled conjugate gradient algorithm for fast supervised learning, *Neural Networks*, **6**, (1993), 525-533.

Norton, S. J. and Linzer, M.: Ultrasonic Reflectivity Imaging in Three Dimensions: Exact Inverse Scattering Solutions for Plane, Cylindrical, and Spherical Apertures, *IEEE Transactions on Biomedical Engineering*, **28**, (1981), 202.

Shattuck, D.P., Weinshenker, M.D., Smith, S.W., and Von Ramm, O.T.: Explososcan: A parallel processing technique for high speed ultrasound imaging with linear phased arrays, *The Journal of the Acoustical Society of America*, **75**, (1984), 1273-1282.

Singanallur, V., Hsiao M.S., Garvin N., Jackson M.A., De Graef M., Simmons J., Bouman C., and Drummy L.F.: Model-based Iterative Reconstruction for Low-dose Electron Tomography, *Microscopy and Microanalysis*, **20**, (2014), 802.

Thibault, J.B., Sauer, K.D., Bouman, C.A., and Hsieh, J.: A three-dimensional statistical approach to improved image quality for multi-slice helical CT," *Medical Physics*, **34**, (2007), 4526–4544.